MAGNETIC RESONANCE IN MEDICINE 9, 139–149 (1989)

Three-Dimensional Phase Contrast Angiography

C. L. DUMOULIN,*† S. P. SOUZA,*† M. F. WALKER,* AND W. WAGLE†

*GE Research and Development Center, Schenectady, New York 12301, and †Albany Medical Center, Albany, New York 12208

Received September 27, 1988

Bipolar flow-encoding gradients can be used in a three-dimensional magnetic resonance imaging procedure to provide a noninvasive measure of *in vivo* blood flow. The resulting volume angiogram is a three-dimensional data matrix which can be retrospectively analyzed and displayed in a variety of ways. This angiographic technique provides good suppression of signals arising from stationary tissue, thereby permitting the visualization of small vessels having relatively slow flow. This suppression is obtained by modulating the amplitude of the flow-encoding gradient pulse to either cancel the stationary tissue signal or displace it relative to the flow signal in the volume image.

INTRODUCTION

The phase shift in transverse spin magnetization induced by spin movement along a magnetic field gradient was first recognized by Hahn (*1*) in 1960. In 1982 the first application of this effect to magnetic resonance imaging was proposed by Moran (*2*). Since then a variety of phase-sensitive flow-imaging procedures has been demonstrated. These have included in-plane techniques in which flow is measured in a relatively thin anatomical section (*3, 4*), and projective techniques in which the flow within a large volume is selectively detected and displayed in angiographic format (*5–9*). In some of these methods, flow is detected as a loss of phase coherence due to velocity dispersions within a vessel (*5, 9*), and in other methods flow is detected as a discrete phase shift (*6–8*).

All phase-sensitive methods of flow measurement have several features in common. First, only the component of velocity which is coincident with a magnetic field gradient will induce a phase shift in transverse spin magnetization. Second, the velocity-induced phase shift is proportional to velocity, and thus dispersions in velocity result in dispersions of phase shifts. This dispersion of phase shifts can result in the attenuation or loss of observable signal when the flow becomes complex or turbulent. Undesired loss of phase coherence can be prevented by employing flow-compensated gradient waveforms (*10*), but the requirements of phase-sensitive flow measurement are incompatible with flow compensation. Another feature of all magnetic resonance angiography methods is that the small size of blood vessels (with respect to the surrounding anatomy) necessitates a high signal-to-noise ratio to provide adequate pixel resolution. Furthermore, complex vessel geometries frequently make the unambiguous assignment of vessels difficult.

0740-3194/89 $3.00

Three-dimensional Fourier transform (3DFT) imaging can be used to circumvent some of the problems of phase-sensitive flow techniques. For example, 3DFT imaging provides a high signal-to-noise ratio for a given scan time because each acquired echo contains signal from all image voxels. Perhaps the most useful aspect of volume imaging for angiographic applications, however, is the ability to unambiguously identify the location of a vessel with respect to its neighbors. Three-dimensional images can be retrospectively analyzed by a variety of mechanisms, some of which are described below. Flow images ideally contain signal from a single type of tissue (i.e., blood) and the restrictions frequently placed on TR, TE, and the rf pulse flip angle to maximize tissue contrast are not relevant.

METHOD

The rf and gradient pulse sequence for three-dimensional phase contrast angiography is shown in Fig. 1. The sequence consists of a limited flip angle excitation rf pulse (typically 10°–30°), a bipolar flow-encoding gradient pulse, and conventional gradient pulse waveforms for the generation of a three-dimensional gradient refocused spin-warp image. The excitation rf pulse is applied simultaneously with a weak slice selection gradient to limit the excitation to the field-of-view and to prevent aliasing of signal into the detection volume. The phase of the rf pulse is held constant during the entire imaging procedure to maintain the stationary spins in a steady state. The flow-encoding gradient pulses are applied in the time period between the rf excitation and the beginning of the image formation gradient pulses. These bipolar gradients are modulated during the imaging procedure to discriminate between signals arising from flowing material and signals arising from stationary tissue. These gradients

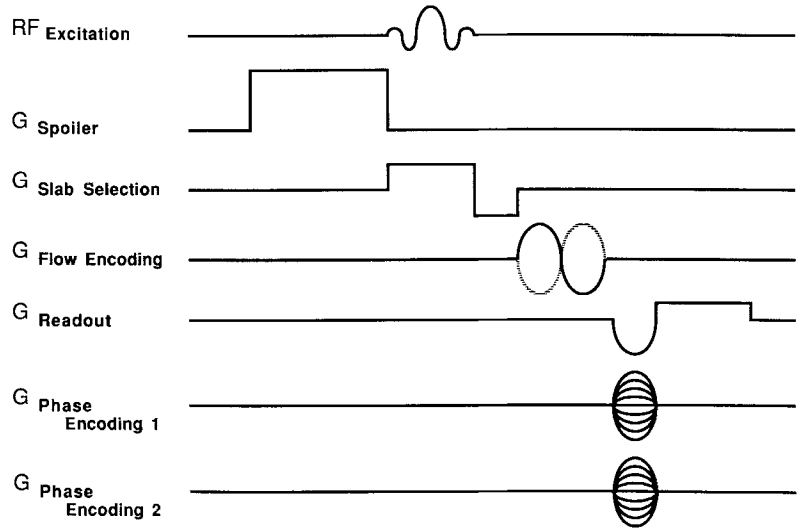

FIG. 1. Radiofrequency and gradient waveforms for 3D phase contrast angiography. In this pulse sequence, the phase of the rf is held constant, and the phases of the flow-encoding gradient pulses are modulated. The flow-encoding gradient pulses are applied on orthogonal axes for each of three exams.

modulate transverse spin magnetization of only those spins which move in the direction of the applied gradient. Consequently, three volume acquisitions must be performed, each sensitive to flow along a unique principal axis. The spin-warp imaging gradient pulses follow the flow-encoding pulses. The phase-encoding and readout-dephasing lobes are placed as close to the acquired echo as possible to prevent velocity dispersion and flow misregistration (*11*) artifacts. The slice select, phase-encoding, and readout gradient waveforms can be flow compensated by the addition of moment nulling waveforms (*10, 11*) but the improvement in image quality may be offset by the resulting increase in TE.

The strategy for processing the data acquired by the pulse sequence described above is outlined in Fig. 2. In this procedure, the three volumes of raw data (one acquired for each primary axis of flow) are first Fourier transformed in three dimensions to obtain the spatial distribution of signal. The magnitude of each complex data point is then calculated to remove the phase information and retain only the amplitude information which is approximately proportional to the flow. The three volumes are now conventional magnitude images, but each contains information from only one of three orthogonal directions of flow. A single volume containing all the flow information can then be generated by combining the three volumes on a voxel-by-voxel basis using the expression

$$M_i = \sqrt{x_i^2 + y_i^2 + z_i^2}, \qquad [1]$$

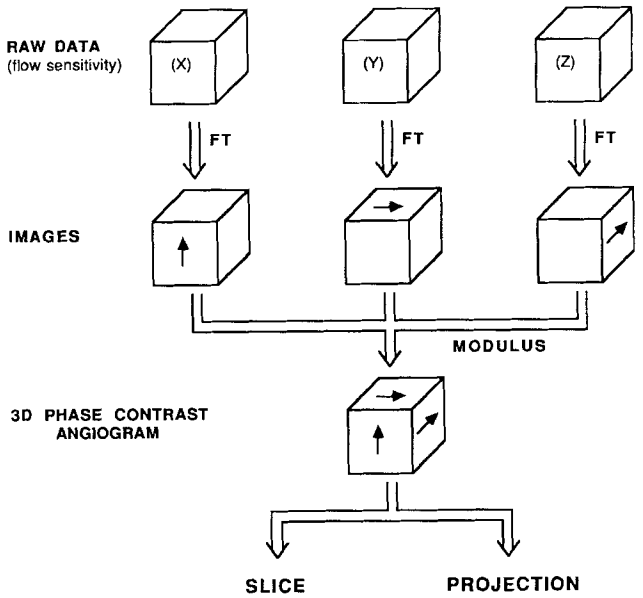

FIG. 2. Processing strategy for 3D phase contrast angiographic data. Three raw data sets are converted into three volume images by three-dimensional Fourier transformation. The magnitudes of these data sets are then combined using a three-parameter modulus function to yield a "total flow" volume angiogram. This angiogram can then be viewed by panning through slices or by the generation of projections.

where M_i is the magnitude of the ith voxel in the final volume and x_i, y_i, and z_i are the voxels containing the x, y, and z components of flow. The resulting volume of data is most conveniently manipulated as a series or stack of two-dimensional images. Images from this series can be viewed individually or in rapid succession. Additional data processing is necessary if an orthogonal stack of images or projections through the volume are desired.

Projections through the three-dimensional volume are a convenient way of reducing the amount of data which must be manipulated while retaining most of its information content. Collapsing the three-dimensional data structure to two dimensions permits viewing the information from the entire volume on two-dimensional display devices such as film and graphics monitors. Angiographic projections are particularly convenient because they resemble X-ray angiographic images. The full utility of projections is not obtained, however, unless the information which is lost in the projection (i.e., depth) is recovered. This can be accomplished with steroscopic image pairs and/or multiple projection images generated at different view angles such that rapid viewing gives the visual impression of the object rotating about a given axis.

Many algorithms can be employed to generate projections from a three-dimensional volume of data. For example, the voxel intensities along a projection ray can be summed to give the integrated projection. Likewise, the maximum voxel intensity encountered along the ray can be used to obtain the maximum pixel projection. The second (or Nth) most intense voxel encountered (or the sum of the most intense voxels) or the standard deviation of all voxel intensities along the projection ray can also be used. The relative worth of these various algorithms depends greatly upon the characteristics of the three-dimensional data and the information which is to be extracted. For the angiography technique presented here we have found that the maximum pixel and standard deviation algorithms provide the best results.

The quality and computational speed of the projection can be enhanced by identifying subvolumes within the data set which contain only artifact, noise, or undesired features. Once these subvolumes have been identified, the voxels within can be ignored in subsequent computations. A second computational mechanism which is useful for improving integrated pixel projections (but is unimportant for maximum pixel projections) is the use of a detection threshold in the projection algorithm. The detection threshold will cause low-intensity voxels to be discarded without affecting the contribution of higher intensity voxels to the projected image. Consequently, low-level features in the image such as incompletely suppressed stationary spin magnetization will not contribute to the resulting projection image. The addition of masks and thresholds to the projection algorithm can improve the quality of the final image, but this improvement comes at the expense of the autonomy of the projection procedure.

EXPERIMENT AND RESULTS

Three-dimensional phase contrast angiography was investigated on a 1.5-T imaging system (GE Medical Systems, Milwaukee, WI). This system was augmented with self-shielded gradient coils (*12*) and a quadrature head coil. Data were obtained in $256 \times 128 \times 128$ matrices. Three matrices were obtained in a study, each sensitive

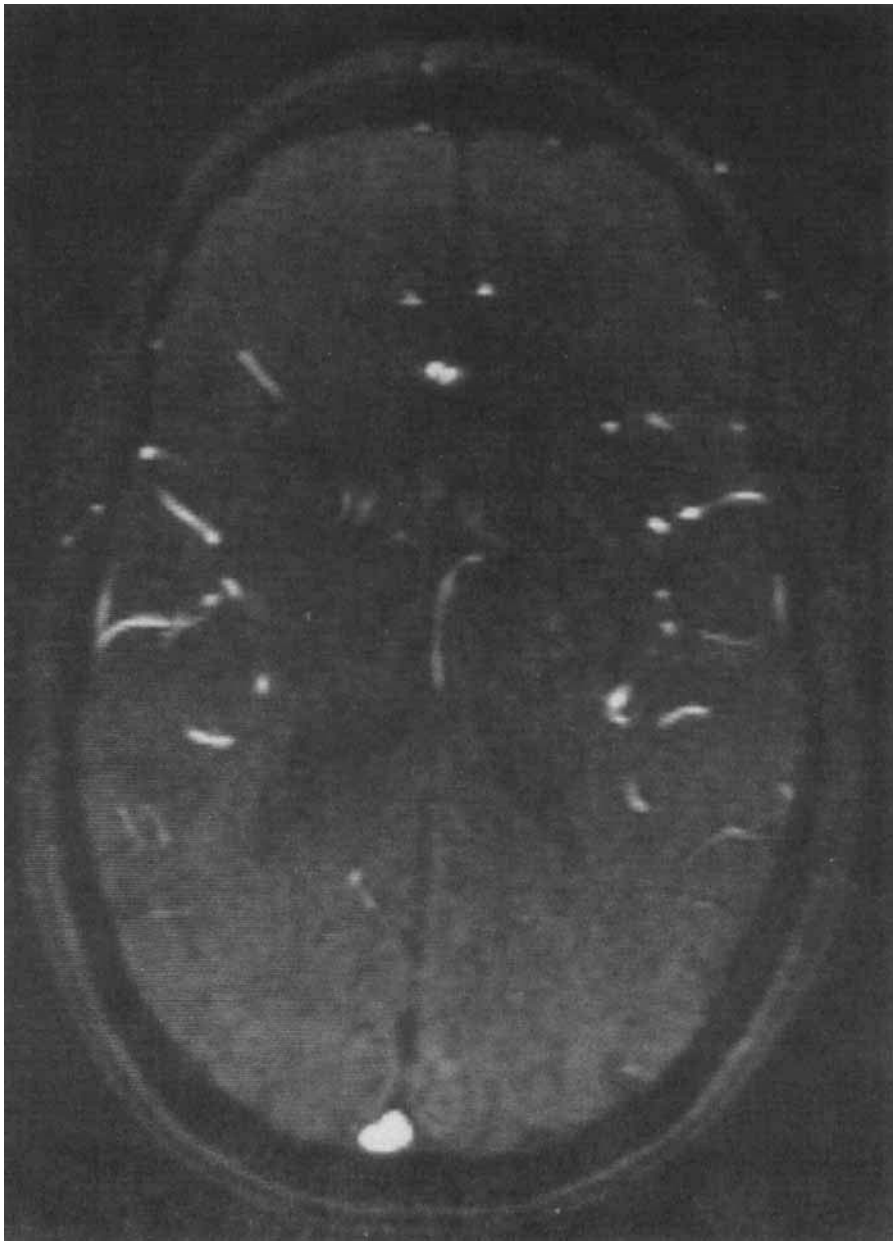

FIG. 3. A 1.9-mm axial slice taken from a 3D phase contrast angiogram of a healthy volunteer.

to flow in one of three orthogonal directions. The field-of-view for a head examination was typically 24 × 24 × 24 cm. Radiofrequency excitation was limited to a 20-cm-thick axial slab. Exams were performed with both NEX = 1 and NEX = 2. The

FIG. 4. Projection of 64 slices superior to and including the basilar artery from the 3D phase contrast angiogram used in Fig. 3, along the patient's inferior–superior axis.

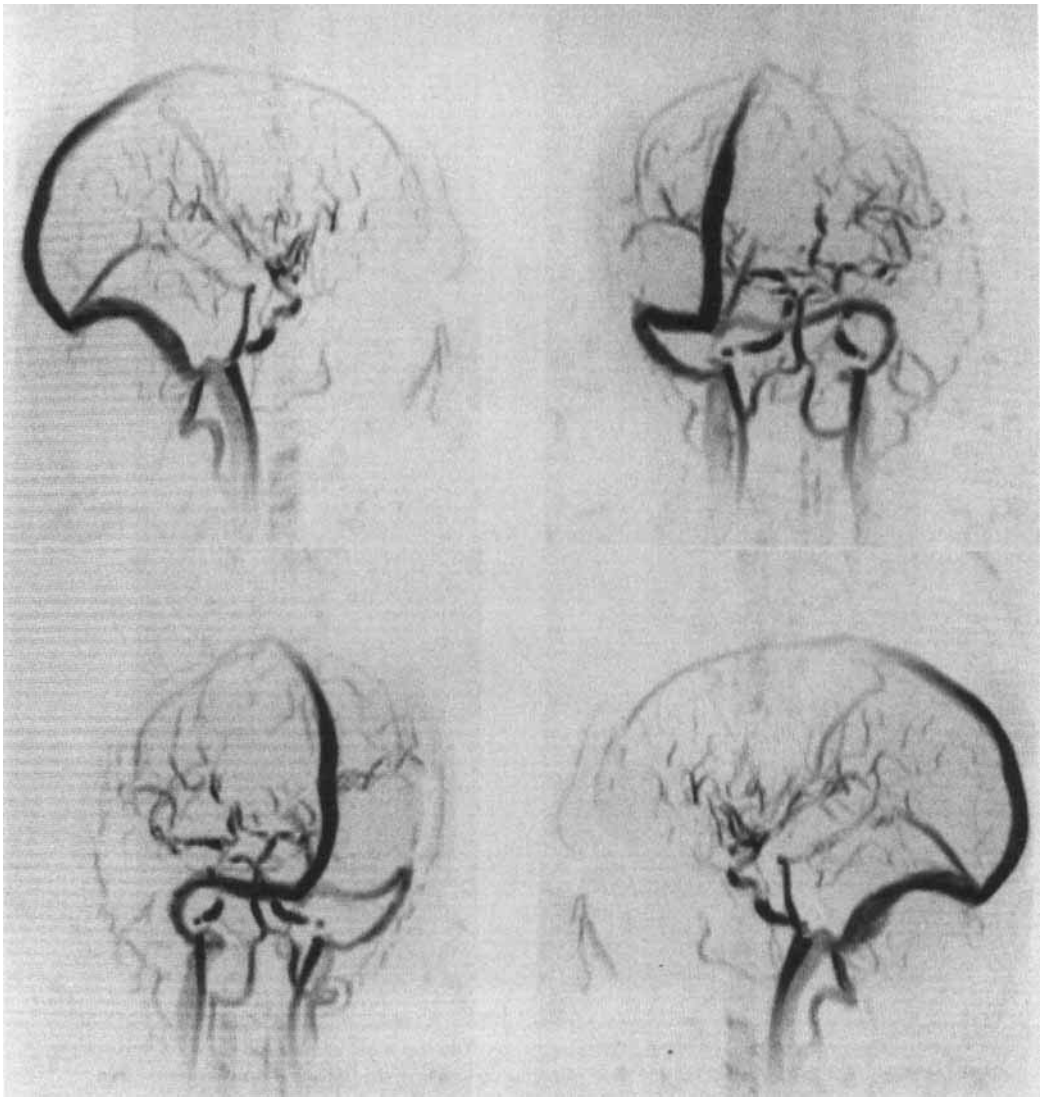

FIG. 5. A set of maximum pixel projections of the data used to generate Figs. 3 and 4.

repetition time, TR, was 23 ms and the echo time, TE, was 15 ms. Total data acquisition time was approximately 37 min for NEX = 2 and 18.5 min for NEX = 1.

Figure 3 is one of 128 axial slices taken from a 3D phase contrast angiography exam on a healthy male volunteer. This image has a slice thickness of 1.9 mm. It is the combination of three flow-sensitive directions as described above. In this image small vessels can be seen entering and exiting the plane of the image. These vessels can be easily followed by viewing adjacent images in rapid succession. Figure 4 is the maximum pixel projection along the patient's inferior–superior axis of 64 axial slices

FIG. 6. Stationary (a) and flow (b) images extracted from a 3D phase contrast angiogram using a NEX = 1 flow-encoding modulation strategy. Both images are from the same anatomical location, but appear displaced by half the field-of-view in the "slice" direction because of the flow-encoding modulation.

from the data set used for Fig. 3. In other words, it represents a 12-cm-thick axial slice. No masks or thresholds were used.

Figure 5 is a set of maximum pixel projections perpendicular to the inferior–superior axis through the three-dimensional volume of data used in Figs. 3 and 4. In these images, a large cylindrical mask whose diameter was equal to the field-of-view was used. This mask is larger than the subject's head and was used only to enhance computational speed.

DISCUSSION

Two strategies for modulation of the flow-encoding gradient pulses have been investigated. The first strategy makes use of a single acquisition at each point in three-

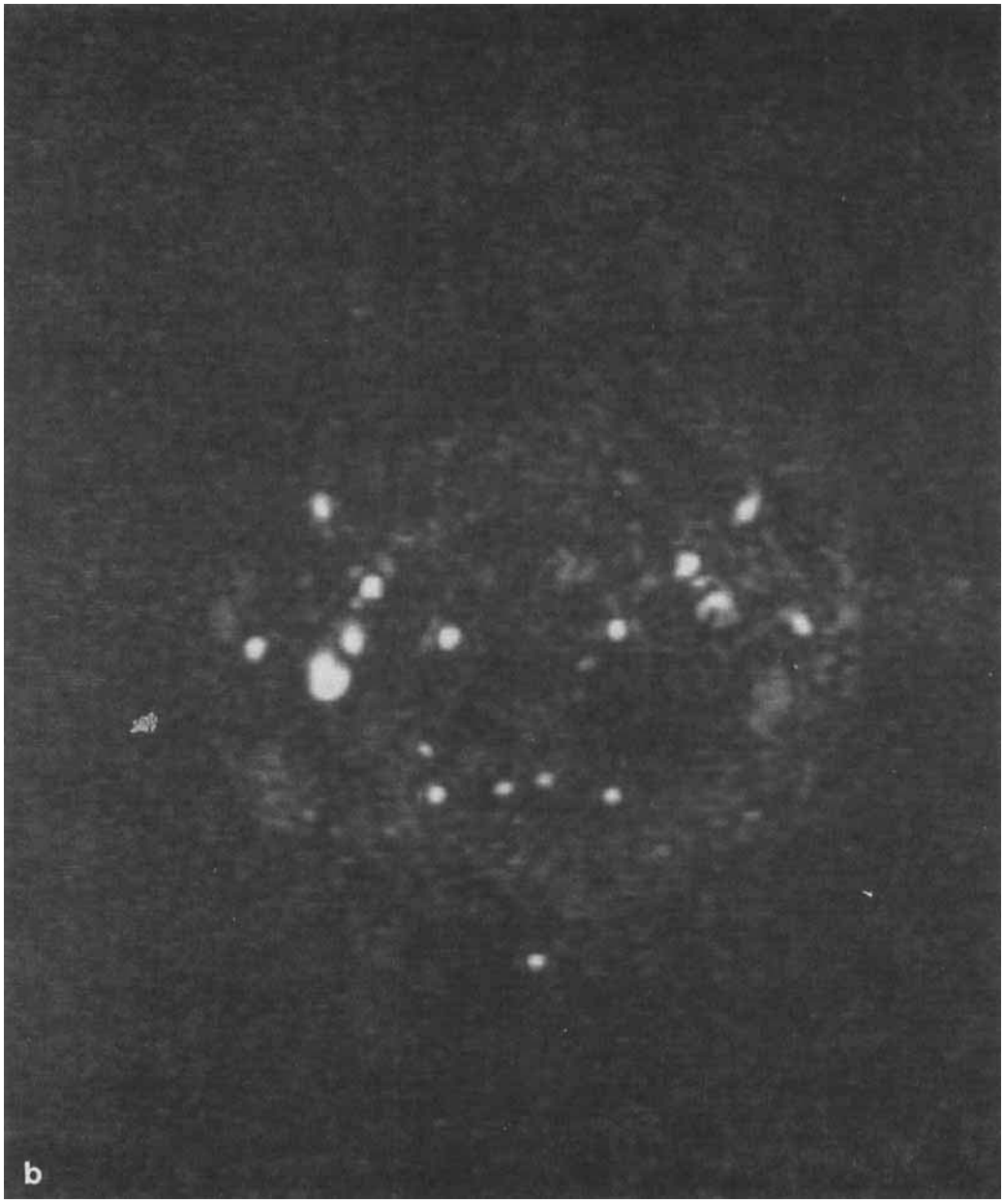

FIG. 6—*Continued.*

dimensional *k* space (i.e., NEX = 1). During the imaging procedure, the phase of the flow-encoding pulse is inverted each time the phase-encoding gradient pulse on one of the axes is advanced. This causes the signals arising from flowing material to be modulated at the sampling frequency in the chosen phase-encoding direction. Conse-

quently, the flow image is displaced by half the field-of-view along the secondary phase-encoding axis, while the stationary spin image is not displaced. This modulation strategy permits the simultaneous detection of both moving blood and stationary tissue as illustrated in Fig. 6. In this case, it is necessary to limit the excitation slab to one-half the field-of-view in the secondary phase-encoding direction to prevent overlap of the flow and stationary spin images.

The second method for modulating the flow-encoding gradient waveforms makes use of an even number of acquisitions at each point in three-dimensional k space (i.e., NEX = 2, 4, 6, . . .). In this technique echoes are obtained with inverted and noninverted flow-encoding pulses for each point in k space. Upon complex subtraction, signal intensity arising from stationary tissue is canceled and signals arising from moving blood are retained. In general the quality of images obtained with this NEX = 2 strategy is better than that of the NEX = 1 image because of greater signal averaging and higher resolution. Presumably, the image quality of NEX = 1 and NEX = 2 image can be made to be identical if the number of phase-encoding steps in the NEX = 1 study is doubled.

In the examples presented above, data from all three orthogonal flow directions are acquired. In clinical situations this amount of data may not be necessary. In many parts of the body, blood flow tends to be along a single axis (usually the patient's inferior–superior axis). Consequently, the three-dimensional acquisition of data could be restricted to a single flow-encoding direction. Such a restriction would drastically reduce the data acquisition and processing times. Unfortunately, blood flow in inappropriately aligned vessels would be impossible to measure.

Three-dimensional phase contrast angiography is well suited to applications in which tortuous vessels having moderate flow are to be imaged over a large field-of-view. For example, the arteries and veins of the head, particularly the posterior branches of the middle cerebral arteries, can be very convoluted and extend over a substantial portion of the brain. This vessel structure is well visualized with three-dimensional phase contrast angiography if all three flow components are obtained. Time-of-flight angiographic methods can be used in this region, but slow flow in the smaller vessels causes the blood to lose its spin label a short distance from the spin labeling region.

While phase contrast angiography may be superior to time-of-flight methods in regions of slow flow and tortuous vessels, phase contrast angiography does have its limitations. The most severe limitation is its sensitivity to pulsatile and nonuniform flow. The sensitivity to pulsatility can be overcome by cardiac gating (*5, 6*) to ensure that the blood velocity is consistent for each acquired echo or by averaging many echoes over the cardiac cycle (*8, 13*) to obtain a measure of average flow. In a three-dimensional phase contrast exam neither option is satisfactory because of exam time constraints. Fortunately, the amount of signal averaging in a three-dimensional exam (even when NEX = 1) appears to be sufficient to attenuate image ghosts due to pulsatility.

A second limitation is the sensitivity of a phase contrast angiography procedure to instrumental imperfections such as eddy currents induced in the cryostat by gradient activity. Inadequate suppression of these eddy currents results in the failure to completely suppress stationary tissue, as seen in Fig. 3. With properly designed self-

shielded gradient coils (*12*) and careful eddy current compensation, three-dimensional angiograms which are devoid of background signals can be routinely obtained. If a low-intensity background image of stationary tissue is desired for anatomical context, the flow-encoding gradients can be intentionally unbalanced to provide any desired mix of stationary and moving signals. Intentionally degrading the suppression of stationary tissue, however, may obscure the slower flowing blood in smaller vessels.

CONCLUSION

Three-dimensional phase contrast angiography is an excellent means of obtaining flow images of complex vessel geometries. The three-dimensional matrix allows for the unambiguous determination of the placement of vessels. Three-dimensional matrices can be retrospectively analyzed in a variety of ways. These include panning through a stack of two-dimensional images which constitute the image volume, and projective techniques in which the three-dimensional data are collapsed into two dimensions by a projection algorithm. In the future, holograms and other three-dimensional image presentations may prove useful for viewing the angiograms.

Three-dimensional phase contrast angiography should find applications in neurological and peripheral angiography. The data acquisition times are similar to those found in current clinical practice (although the data processing requirements are significant). Applications in which the blood flow is highly pulsatile and/or turbulent are not likely to be addressed by this technique. Nevertheless, the three-dimensional phase contrast technique should prove clinically useful for many applications in neurological and peripheral angiography.

REFERENCES

1. E. L. HAHN, *J. Geophys. Res.* **65,** 776 (1960).
2. P. R. MORAN, *Magn. Reson. Imaging* **1,** 197 (1982).
3. M. O'DONNELL, *Med. Phys.* **12,** 59 (1985).
4. P. R. MORAN, R. A. MORAN, AND N. KARSTAEDT, *Radiology* **154,** 433 (1985).
5. V. J. WEDEEN, R. A. MEULI, R. R. EDELMAN, *et al., Science* **230,** 946 (1985).
6. C. L. DUMOULIN AND H. R. HART, *Radiology* **161,** 717 (1986).
7. C. L. DUMOULIN, S. P. SOUZA, AND H. R. HART, *Magn. Reson. Med.* **5,** 238 (1987).
8. C. L. DUMOULIN, S. P. SOUZA, M. F. WALKER, *et al., Magn. Reson. Med.* **6,** 275 (1988).
9. G. A. LAUB AND W. A. KAISER, *J. Comput. Assist. Tomogr.* **12,** 377 (1988).
10. Q. S. XIANG AND O. NALCIOGLU, "5th Annual Meeting of Society of Magnetic Resonance in Medicine," p 100, 1986.
11. C. L. DUMOULIN, S. P. SOUZA, M. F. WALKER, AND W. WAGLE, *Magn. Reson. Med.*, in press.
12. P. B. ROEMER, W. A. EDELSTEIN, AND J. S. HICKEY, "5th Annual Meeting of the Society of Magnetic Resonance in Medicine," p. 1067, 1986.
13. E. M. HAACKE, G. W. LENZ, AND A. D. NELSON, *Magn. Reson. Med.* **4,** 162 (1987).